Atomic Layer Deposition of a Silver Nanolayer on Advanced Titanium Orthopedic Implants Inhibits Bacterial Colonization and Supports Vascularized de Novo Bone Ingrowth

*Aine Devlin-Mullin, Naomi M. Todd, Zahra Golrokhi, Hua Geng, Moritz A. Konerding, Nigel G. Ternan, John A. Hunt, Richard J. Potter, Chris Sutcliffe, Eric Jones, Peter D. Lee, and Christopher A. Mitchell**

Dedicated to the memory of a great friend and colleague; Prof. Moritz A. Konerding: 22nd April 1960–26th January 2015

Joint replacement surgery is associated with significant morbidity and mortality following infection with either methicillin-resistant *Staphylococcus aureus* (MRSA) or *Staphylococcus epidermidis*. These organisms have strong biofilm-forming capability in deep wounds and on prosthetic surfaces, with 10^3–10^4 microbes resulting in clinically significant infections. To inhibit biofilm formation, we developed 3D titanium structures using selective laser melting and then coated them with a silver nanolayer using atomic layer deposition. On bare titanium scaffolds, *S. epidermidis* growth was slow but on silver-coated implants there were significant further reductions in both bacterial recovery ($p < 0.0001$) and biofilm formation ($p < 0.001$). MRSA growth was similarly slow on bare titanium scaffolds and not further affected by silver coating. Ultrastructural examination and viability assays using either human bone or endothelial cells, demonstrated strong adherence and growth on titanium-only or silver-coated implants. Histological, X-ray computed microtomographic, and ultrastructural analyses revealed that silver-coated titanium scaffolds implanted into 2.5 mm defects in rat tibia promoted robust vascularization and conspicuous bone ingrowth. We conclude that nanolayer silver of titanium implants significantly reduces pathogenic biofilm formation in vitro, facilitates vascularization and osseointegration in vivo making this a promising technique for clinical orthopedic applications.

1. Introduction

Total hip replacements (THR) generally have an excellent clinical outcome; however, perioperative infection rates following this procedure range from 0.5% to 2%[1] and with over 62 000 of these surgeries performed each year in the UK (National Joint Registry, 2014) there is an urgent clinical need to reduce biofilm formation on the surface of materials used in these devices. THR infection usually results in two additional surgical procedures: one to remove the implant and eradicate the infection followed by an additional THR. This treatment puts a significant burden on the patient and health service resources, as revision surgery can be up to three to four times the cost of the initial THR.[2] There are several risk factors, which can increase the possibility of implant related infection, including increased operative time,[3] comorbidities, and a prior history of a joint arthroplasty.[4]

Infections following THR can be caused by very low numbers (10^3–10^4) of osteolytic

A. Devlin-Mullin, N. M. Todd, Dr. N. G. Ternan, Prof. C. A. Mitchell
Centre for Molecular Biosciences (CMB)
School of Biomedical Sciences
Ulster University
Coleraine BT521SA, UK
E-mail: ca.mitchell@ulster.ac.uk

Dr. Z. Golrokhi, Dr. R. J. Potter, Prof. C. Sutcliffe, Prof. E. Jones
School of Engineering
University of Liverpool
Liverpool L69 3GH, UK

Dr. H. Geng, Prof. P. D. Lee
School of Materials
The University of Manchester
Oxford Rd, Manchester M13 9PL, UK

Prof. M. A. Konerding
Institute of Functional and Clinical Anatomy
Johannes Gutenberg University
Mainz 55128, Germany

Prof. J. A. Hunt
Institute of Ageing and Chronic Disease
University of Liverpool
Liverpool L7 8TX, UK

DOI: 10.1002/adhm.201700033

The copyright line for this article was changed on 21 Mar 2017 after original online publication.

This is an open access article under the terms of the Creative Commons Attribution License, which permits use, distribution and reproduction in any medium, provided the original work is properly cited.

microorganisms and are mainly attributable to coagulase negative staphylococci, Gram-negative rod-shaped bacteria, and streptococci.[1,4] Implant-related infections are caused by microorganisms, which colonize and form biofilms on the implant surface, and infection occurs in three main ways: microbial colonization at the time of implantation; hematogenous spreading of the pathogen to the implant; or via direct spreading from an adjacent infection.[5] When microbial pathogens adhere to the implant they form a complex biofilm, which provides protection for the constituent organisms from both the host's immune system and from the penetration of antibiotics.[6] The process of colonization of an implant is described as a "race for the surface" between the host cells, bone extra cellular matrix, and the microbial pathogen.[7]

With the onset of an osteolytic infection, there are many problems for the patient: including primarily, pain, increased risk of hospitalization, additional surgical procedures, and poor functional outcome.[8] Treatment options will depend on the health of the patient, the extent of the infection, debridement of infected tissue around the joint, and retention of a well fixed prosthesis. The two main treatment options are: one-stage revision surgery, consisting of the removal of the prosthesis, infected tissue and cement with reimplantation of a new prosthesis; or alternatively, two-stage revision surgery, where reimplantation of the prosthesis is delayed for 6–8 weeks and antibiotic eluting cement spacers are used to combat infection. Bone cements loaded with antibiotics are still in use but the extensive use of gentamicin as well as increasing antibiotic resistance means further infection prevention measures are required to lower the incidence of clinically relevant perioperative hip infections.[9,10] Two-stage revisions are the most common approach to treat chronic prosthetic joint infections in many hospitals, but in severe cases where the patient is unsuitable for surgery and antibiotics are not effective, hip disarticulation may be considered.[11]

Titanium is a commonly used material for orthopedic applications and additive manufacturing techniques are now widely used[12] to create the complex geometries required for orthopedic applications such as THR. In addition to complex geometry, the surfaces of these titanium structures have the potential for modification by a variety of methodologies, including introduction of biomimetic molecules[13,14] and anionic plasma chemical approaches.[15] These techniques can introduce surface modifications that enhance biocompatibility[14] and improve biomechanical properties[12] or decrease bacterial adhesion[16] and growth, thus reducing the potential for infection.[17] The prevention of osteolytic infections is a high priority in the field of orthopedic research and has been widely explored with approaches including the coating of titanium implants with various metallic and organic compounds, and impregnation of bone cement with silver[18] or antibiotics.[19] The use of silver as an antimicrobial agent dates to around 4000BC in ancient Egypt[20] and it is still used today as a microbicide as it kills a broad range of microorganisms,[21] although in vitro resistance in *Escherichia coli* and has been noted in organisms with metal ion-transport pump deficiencies.[22] Silver coatings have previously been used in the field of orthopedics on a variety of implantable devices such as catheters, where they have been shown to reduce bacterial associated urinary tract infections.[23,24] In the past, polymethyl methacrylate bone cement was loaded with silver but this was found to cause serious side effects. In human trials, neurological deficits and muscle paralysis due to the silver accumulation within the central nervous system were observed.[18]

As the therapeutic range of silver is relatively narrow, it is critical to minimize the amount of silver in order to prevent cytotoxicity while still retaining sufficient antibacterial activity.[25] Therefore, we sought to develop orthopedic implants with ultrathin nanosilver coatings that exhibit none of this cytotoxicity while at the same time maintaining a high effectiveness against multidrug-resistant bacteria.[9] Others have previously reported on the use of nanosilver coatings and while some report positive antimicrobial results, there often remains a significant disconnect between the science and the "real world" manufacturability of coated implants. Techniques such as plasma immersion ion implantation[26] have been used to embed silver-nanoparticles into titanium and show that these modified surfaces are highly effective in inhibiting *Staphylococcus aureus* and *E. coli* strains while promoting in vitro proliferation of osteoblast-like cells.

While plasma-based surface treatments are readily applied to flat substrates, they are often limited to line-of-sight treatments as plasma species decay over time, particularly as they interact with surfaces. As with plasma-based processes, physical vapor deposition (including evaporation, sputtering, pulsed laser deposition, and molecular beam epitaxy) processes also suffer from line-of-sight limitations, which limits their usefulness for coating the complex 3D geometries associated with porous orthopedic implants. In the current study, we use atomic layer deposition (ALD) to produce ultrathin, highly conformal silver films on 3D bone-like titanium implants.

ALD is an adaptation of chemical vapor deposition, which uses self-limiting surface reactions that offer a number of key benefits over many of the other coating methods available. These benefits include subangstrom thickness control, which is controlled "digitally" using the number of ALD cycles, extremely high conformality (even on very high aspect ratio 3D structures), batch processing compatibility so that large numbers of different shape and size implants can potentially be coated simultaneously and highly repeatable processing control. Therefore, ALD is capable of yielding a uniform deposition[27] of silver on complex structures such as the foams and solids described in this study.[28]

The technological development of the selective laser melting (SLM) technique[29] allows production of functionally graded parts for orthopedic applications. SLM enables titanium orthopedic implants to be generated with intricate geometries, where solid and porous structures are contiguous. Porous structures with optimized pore sizes in the range of 100–700 µm are required to encourage bone ingrowth into certain areas, while solid components provide greater biomechanical strength for the bony attachment of the prosthesis. In order to reduce the potential for silver toxicity while maintaining bactericidal properties of the surface of SLM manufactured implants, we coated our titanium structures with a nanolayer of metallic silver using ALD.

When examining the biological properties of surface layering of titanium with silver or silver composites, the bactericidal

 © 2017 The Authors. Published by WILEY-VCH Verlag GmbH & Co. KGaA, Weinheim

potential in conjunction with its in vitro[30] and/or in vivo [reviewed in ref. [31]] abilities to facilitate bone growth is rarely investigated[14]; this makes the assessment of the potential clinical applications for these coating techniques problematic. Therefore, the purpose of our unique biological investigations was threefold: to determine the microbicidal effect of a conformal-nanolayer ALD-deposited silver on implants in the presence of clinically relevant osteolytic bacterial strains (*Staphylococcus epidermidis* ATCC 35983 and methicillin-resistant *Staphylococcus aureus* (MRSA) ATCC 43300): to investigate the influence of surface modification on cell growth in vitro and, most critically, to confirm that the new blood vessels, which ensure tissue survival, grow within the regenerated bone.

2. Results

2.1. Production of Ti-Only or Ti/Ag Scaffolds for In Vitro and In Vivo Studies

Ultrastructural examination of the samples revealed uniform solid (**Figure 1**a,c) and 30° randomized tetrahedral foam scaffolds (Figure 1b,d) characterized by a roughened surface topology, with varying numbers of 30–50 µm diameter nodules (incipiently melted Ti powder) on their surfaces. Low magnification ultrastructural examination revealed that surface topology of the Ti samples is smooth (Figure 1a,b), whereas the surface morphology of Ti–Ag scaffolds (Figure 1c,d) exhibited a grainy texture.

2.2. Characterization of Nanolayer Silver Surface Coating of Titanium

Self-limiting ALD growth conditions for the silver process were established prior to the current work and are reported elsewhere.[28] As with other ALD processes, under self-limiting conditions, the total mass deposition increases in a linear fashion with ALD cycles (**Figure 2**a). There appears to be a slight deviation from this for low numbers of cycles, which is attributed to the nucleation of the growth. If the films are assumed to be planar with a density equal to the bulk value of silver (10.49 g cm^{-3}), then the mass deposition after 500 cycles would equate to film thickness of ≈13 nm. The X-ray diffraction (XRD) pattern (Figure 2b) of ALD silver deposited on Si(100) shows reflections at 2θ values of 38.2° and 44.4°, which are consistent with the (111) and (200) features of metallic silver with the (Fm-3m) space group (JCPDS 04-0783).

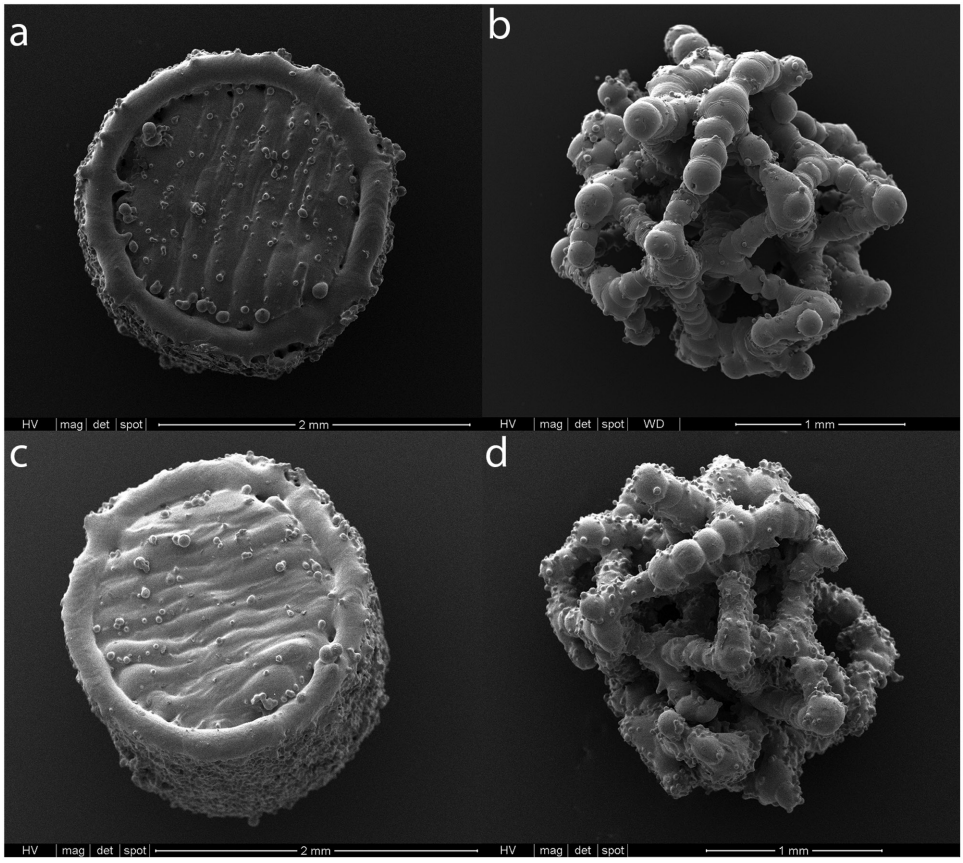

Figure 1. Two types of structures: solid (left panel: a & c) or 30° randomized tetrahedral foams (right panels; b & d) were generated by SLM followed by sintering. Approximately half the samples were used as Ti-only controls (top panel; a & b) or titanium coated with a nanolayer of silver (bottom panel; c & d). For microbiological and cell culture studies solid samples were used, whereas foam samples were used for in vivo studies to facilitate ingrowth of regenerating bone into the porous structure.

 © 2017 The Authors. Published by WILEY-VCH Verlag GmbH & Co. KGaA, Weinheim

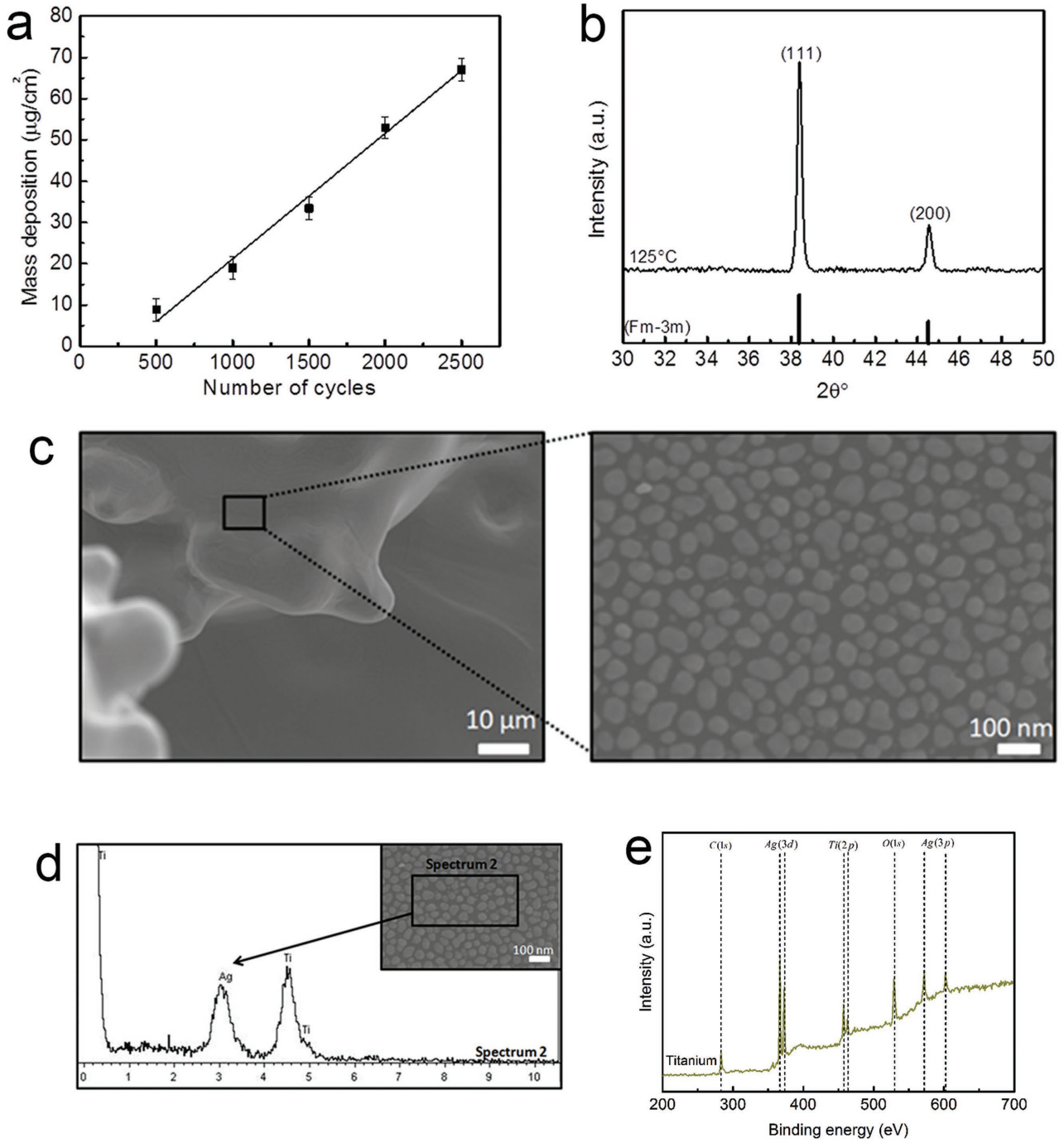

Figure 2. Growth and physicochemical characterization of ALD silver at 125 °C. Mass deposition per unit area as a) a function of ALD cycles performed at 125 °C on flat titanium foil. b) X-ray diffraction of ALD silver deposited at 125 °C with 500 ALD cycles on silicon. c) High-magnification SEM images reveals silver nanoparticles deposited on a titanium porous substrate. d) Energy-dispersive X-ray spectroscopic characteristic spectrum obtained for silver-nanoparticles deposited on titanium substrate; the observable peaks confirm the presence of silver and titanium in the sample. e) XPS spectrum of silver deposited on a flat titanium foil.

Scanning electron microscopy (SEM) analysis of the silver films deposited on titanium (Figure 2c) reveals that the films are textured at the nanoscale. For films deposited using 500 cycles, the nanoparticles tend to be nonsymmetrical and vary in size between ≈40 and ≈90 nm. More detailed studies, which will not be reported here, show that growth proceeds by a process of nucleation and growth of uniformly sized hemispherical nanoparticles. However, as the nanoparticles grow with increasing numbers of ALD cycles, individual nanoparticles merge together to form irregular nanostructures. Energy-dispersive X-ray (EDX) of the films (Figure 2d) shows two clear peaks at ≈3 and ≈4.5 keV, which correspond to the L_{α}-emission line of silver and

 © 2017 The Authors. Published by WILEY-VCH Verlag GmbH & Co. KGaA, Weinheim

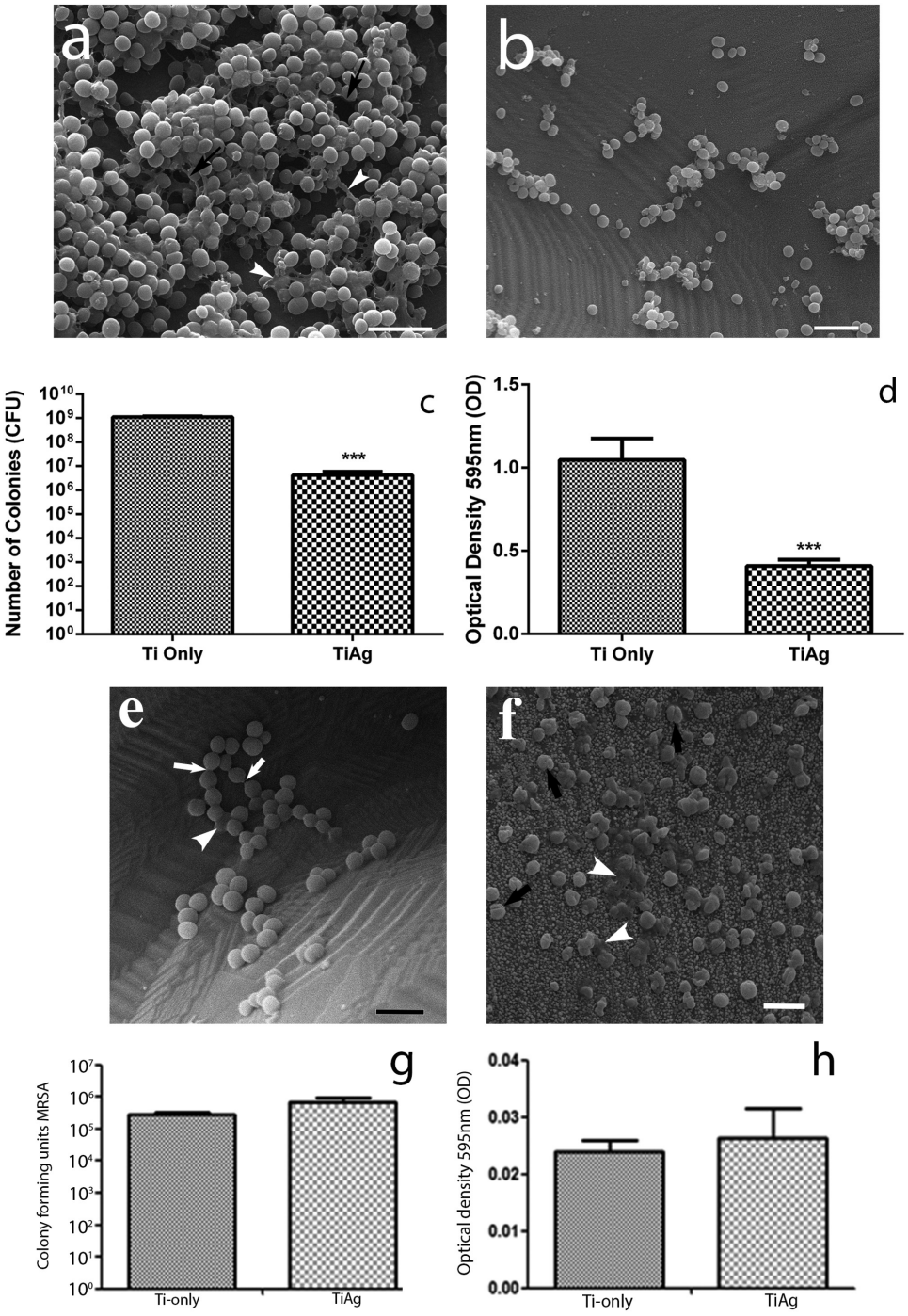

Figure 3. a) Ultrastructural examination of a Ti-only sample, reveals a multilayered *S. epidermidis* biofilm resulting from incubation of 10^3 organisms for 96 h. Several water pores (black arrows) and threadlike appendages between organisms (arrowheads), both typical of biofilms are observed. On Ti/Ag solids b) the surface density of organisms is markedly reduced compared to Ti-only samples. Bars = 5 mm. Quantitative studies revealed a > 2-log reduction in c) c.f.u. numbers of *S. epidermidis* d) as well as reduced crystal violet elution in Ti/Ag samples when compared with Ti-only controls. Scanning electron microscopic examination of MRSA cultured for 96 h on either e) Ti-control or f) Ti/Ag scaffolds revealed relatively few organisms on the materials' surfaces, although there is evidence of replication (arrows), in addition to deposition of mucoid-like matrix (arrowheads). No statistically significant differences in c.f.u. numbers were detected on either g) scaffold type, although there was a 2–3-log reduction in growth when compared to *S. epidermidis* cultures (cf. Figure c). There were also no differences in crystal violet quantitation (NS; $p > 0.05$) from MRSA cultures grown on h) either Ti-only or Ti/Ag scaffolds; although these values were much lower than those observed in *S. epidermidis* cultures (cf. Figure d). Graphs show a single representative data set ($n = 6$) from three independent experiments, with columns indicating mean ± SEM. Statistical significance was assessed with a student's *t*-test; ***$p < 0.001$.

 © 2017 The Authors. Published by WILEY-VCH Verlag GmbH & Co. KGaA, Weinheim

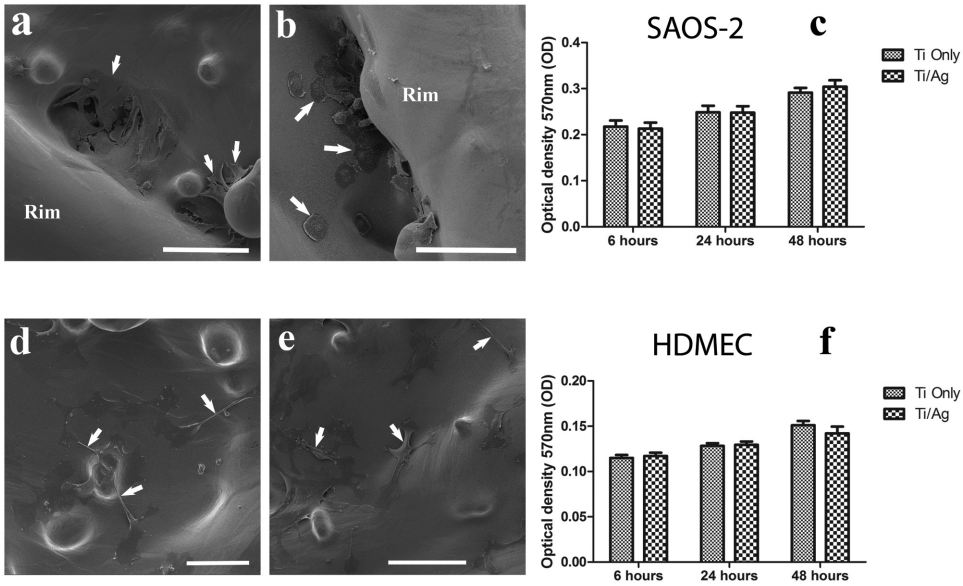

Figure 4. a–c) SAOS-2 osteosarcoma and d–f) HDMEC-1 endothelial cells grow on the surface of either Ti-only or Ti/Ag scaffolds. After 24 h of culture, SAOS-2 cells with characteristic squamous morphology were observed to be tightly adherent, closely apposed and found in clusters, particularly near the rim of solid scaffolds of both a) Ti-only and b) Ti/Ag samples. There was a gradual increase in cell viability of c) SAOS-2 cells from 6 to 48 h ($p < 0.05$) but no differences in viability between those seeded on either Ti or Ti/Ag scaffolds (NS; $p > 0.05$). HDMEC grown on the surface of either d) Ti-only or e) Ti/Ag scaffolds are typically found in small clusters, with some cells showing elongated lamellipodia spanning surface depressions (arrows). In HDMEC cultures, results from MTT assays indicated that there was a gradual increase in cell viability from 6 to 48 h ($p < 0.05$) but no statistically significant difference between OD_{575} values from Ti-only or Ti/Ag scaffolds (NS; $p > 0.05$).

k_α-emission line of titanium, respectively. To confirm that the ALD does not leave behind precursor residue, X-ray photoelectron spectroscopy (XPS) was carried out on a titanium witness sample (Figure 2e). Features relating to silver, titanium, carbon, and oxygen are visible, but no fluorine feature is observed (the F1s feature would be at ≈688.8 eV). The binding energies of the carbon and oxygen features are consistent with atmospheric surface absorbates such as water, carbon monoxide, and carbon dioxide.[28] The absence of a fluorine feature in the XPS provided evidence that the ALD reaction is clean and proceeds to completion.[28]

2.3. Growth of *S. epidermidis* and MRSA on Silver-Coated Titanium Structures

Bacterial adhesion and biofilm formation on both uncoated and silver-coated titanium structures were investigated by ultrastructural examination and determination of colony forming units (c.f.u.) of scaffolds seeded with $\approx 1 \times 10^3$ cells of either *S. epidermidis* (**Figure 3**a–d) or MRSA (Figure 3e–h) on their surfaces for 96 h. Ultrastructural features of *S. epidermidis* biofilm formation on titanium scaffolds, included multilayered coccoid structures within a mucoid-like matrix containing water pores (Figure 3a), whereas Ti/Ag scaffolds had much fewer of these organisms on their surface and showed little evidence of biofilm formation at 96 h (Figure 3b). In addition, a 2-log reduction in the numbers of *S. epidermidis* organisms recovered from silver-coated titanium solids ($p < 0.001$) was consistently observed (Figure 3c). Following solubilization of crystal violet (CV) (a quantitative measure of biofilm formation), solutions obtained from silver-coated titanium structures seeded with *S. epidermidis* also had a significantly lower optical density (OD) when compared to uncoated samples (Figure 3d; $p < 0.001$). Growth of MRSA on either Ti-only samples (Figure 3e,g,h) was slow in comparison to that observed by *S. epidermidis* (cf. Figure 3a,c,d). However, early indications of biofilm formation by MRSA were observed on both Ti-only and Ti/Ag scaffolds at 96 h (Figure 3e,f); although neither c.f.u. counts (Figure 3g) nor spectrophotometric measurements for ODof crystal violet staining of biofilms (Figure 3h) were significantly different (NS; $p > 0.05$).

2.4. Human Cell Lines Attach and Grow on Silver-Coated Titanium Scaffolds

Ultrastructural analysis of a primary human osteogenic sarcoma cells (SAOS-2) with osteoblast-like phenotype grown for 48 h on either Ti-only (**Figure 4**a) or Ti/Ag (Figure 4b) scaffolds revealed that both implant types contained clusters of adherent cells with typically squamous morphology. Assays employing 3-(4,5-dimethylthiazol-2-yl)-2,5 diphenyltetrazolium bromide (MTT) also confirmed that from 6 to 48 h SAOS-2 cell viability increased ($p < 0.05$; Figure 4c), although there were no statistically significant differences between growth on either Ti-only or Ti/Ag scaffolds (NS; $p > 0.05$). Following incubation for 48 h, human microvascular endothelial cells (HDMEC) with typical bipolar morphology and exhibiting filopodial and lamellipodial

 © 2017 The Authors. Published by WILEY-VCH Verlag GmbH & Co. KGaA, Weinheim

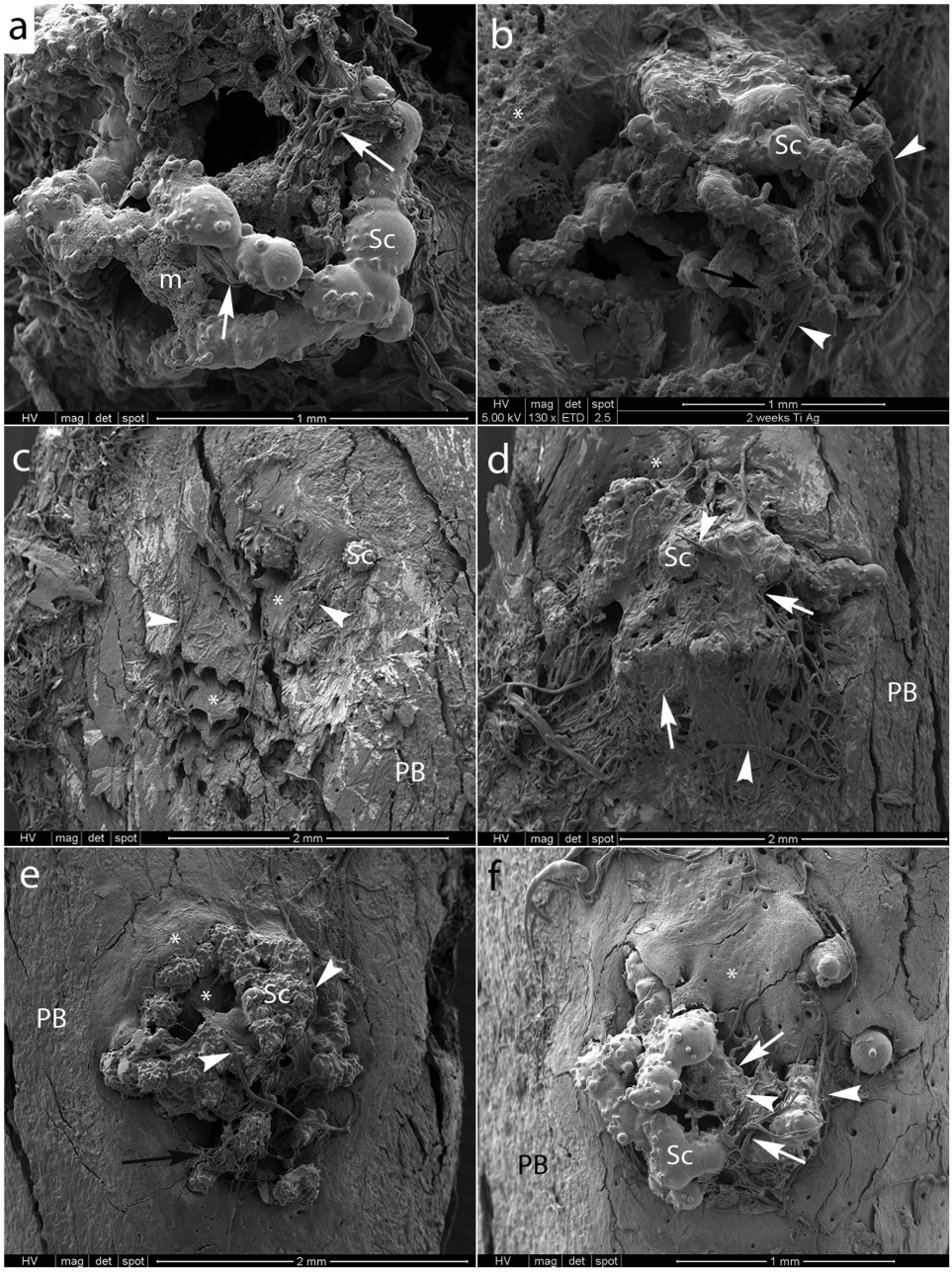

Figure 5. Robust bone and microvascular ingrowth is observed in both Ti-only and Ti/Ag foam scaffolds. Rat tibial subcritical size defects were implanted with either a,c,e) un-coated or b,d,f) Ti/Ag-coated foams and animals recovered from surgery for either a,b) 2, c,d) 6, or e,f) 12 weeks. Animals were then perfused with vascular casting resin, the tibiae dissected, the soft-tissue removed by desiccation and samples prepared for imaging by scanning electron microscopy. At 2 weeks in both a) Ti and b) Ti–Ag samples, there is new bone growth at the periphery and mineralized material on struts but relatively little new bone within the scaffold pores; robust ingrowth of larger caliber vessels (arrowheads) as well as capillaries is conspicuous around the struts (arrows). At the edge of the foams early bone ingrowth is evident (asterisk), while around the struts copious filamentous material and mineral deposition is seen. After 6 weeks in vivo, the foams were infiltrated with porous bone (asterisks) covered by a fibromatrix with dispersed crystalline mineral deposits. After 12 weeks e,f) in vivo, there was evidence of compact bone ingrowth (asterisks) into the pores of both e) Ti-only and f) Ti/Ag implants and microvascular architecture around the struts was more organized with fewer anastomoses (cf. 2 weeks). Volkmann canals (many with attending capillaries) were observed both at the edges of the implants as well as within the pore structures. Cracks on the specimens and separation of regenerated bone (particularly around struts) is an artifact of processing for SEM. PB, pre-existing bone; Sc, scaffold; asterisk, new bone growth; m, mineralized matrix.

extensions were observed on either Ti (Figure 4d) or Ti/Ag scaffolds (Figure 4e). MTT assay analyses revealed that cell viability of surface associated with HDMEC cells also increased from 6 to 48 h ($p < 0.05$; Figure 4f), although there were no significant differences between the Ti and Ti/Ag groups (NS; $p > 0.05$).

 © 2017 The Authors. Published by WILEY-VCH Verlag GmbH & Co. KGaA, Weinheim

2.5. Detection of Free Ag by Inductively coupled plasma mass spectrometry (ICP-MS)

ICP-MS reading from samples of liver taken from animals implanted with either Ti-only or Ti/Ag-coated implants, resulted in readings that were at or below the limit of detection (1 part per billion), indicating that there is no detectable Ag/Ag^+ in these samples.

2.6. Vascular Corrosion Casting and Ultrastructural Analysis

Ultrastructural analyses of vascular corrosion casts from rat tibiae implanted with either Ti-only (**Figure 5**a,c,e) or Ti/Ag (Figure 5b,d,f) foam scaffolds revealed the relationship between pre-existing bone, as well as morphology of microvasculature at 2 (Figure 5a,b), 6 (Figure 5c,d), and 12 weeks (Figure 5e,f) following surgery. At 2 weeks, the foam scaffolds were infiltrated at their edges with a highly porous bone matrix and a dense network of microvessels (particularly around the struts) that originated from pre-existing bone surrounding the site of the defect (Figure 5a,b). Conspicuous mineralized material also encrusts the struts on the surface of Ti-only and Ti/Ag scaffolds at 2 weeks (Figure 5a,b). Ultrastructural examination of the surface of a 2 week Ti/Ag implant revealed hemitubular structures in various stages of development (**Figure 6**), which were characterized by concentric lamellae and contained mineralized, parallel-orientated fibril bundles (inset of Figure 6); features that are consistent with de novo Haversian system formation. In 6 week samples, the gaps within scaffolds of both Ti-only and Ti/Ag foams contained numerous blood vessels interspersed with porous bone or partially ossified fibrous material (Figure 5c,d). Ultrastructural analyses of vascular casts from rat tibia harvested at 12 weeks following implantation with Ti-only or Ti/Ag foams showed that implants were infiltrated with bone containing Volkmann canals with attendant microvessels (Figure 5e,f). Microvessel morphology from tibiae implanted with Ti-only or Ti/Ag scaffolds and harvested at 12 weeks were more regular, smooth and had fewer anastomoses with neighboring vessels than those observed in 2 week samples (cf. Figure 5e,f with Figure 5a,b).

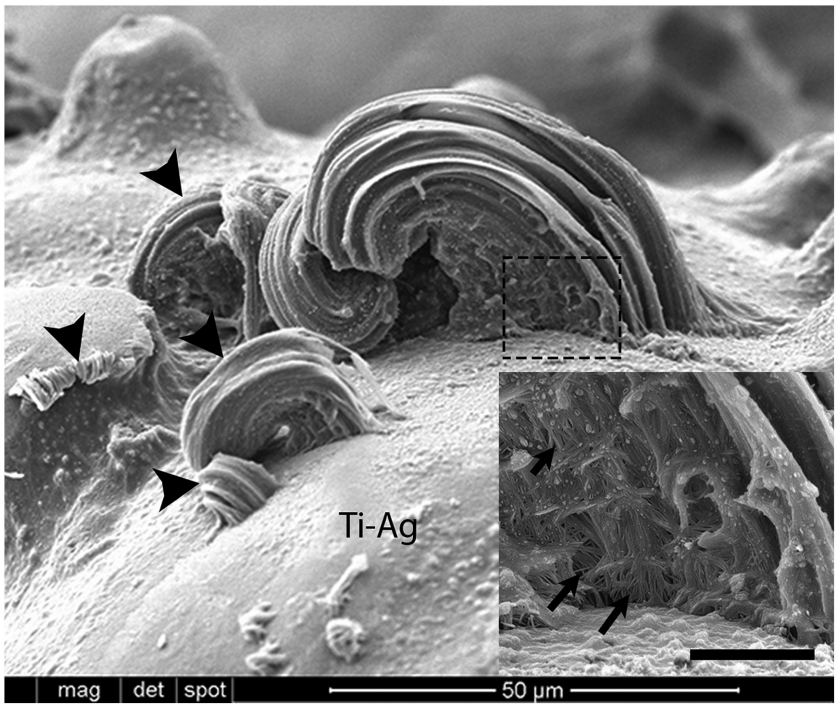

Figure 6. Scanning electron microscopy revealed conspicuous mineralized, hemitubular structures (arrowheads) attached to the surface of a Ti/Ag-coated foam scaffold implanted for 2 weeks in a rat tibia. At higher magnification (inset from boxed area; bar = 5 µm), one of these structures exhibits aligned and mineralized fiber bundles (arrows) within concentric lamellae; structures that are consistent with formation of an early Haversian system directly on the material.

2.7. Histology

Light microscopic examination of thick (50–100 µm) sections from rat tibiae sampled at 2 weeks post-implantation revealed infiltration of porous woven bone at the edges and core of both Ti-only (**Figure 7**a) and Ti/Ag scaffolds (Figure 7b). By 12 weeks, compact bone ingrowth was observed throughout the scaffolds in both Ti-only (Figure 7c) and Ti/Ag (Figure 7d) scaffolds in close apposition to the struts.

2.8. X-ray Microtomographic (XMT) Analysis of Scaffolds In Vivo

The percentage of bone ingrowth (BI) at 12 weeks and statistical significances for these values are presented in **Figure 8**. Postimplantation, Ti or Ti/Ag scaffolds appear well incorporated into 2.5 mm defects in rat tibiae at all timepoints, demonstrating robust bone ingrowth. A conspicuous amount of bone ingrowth is observed between 2 and 12 weeks. At 12 weeks postimplantation, Ti (Figure 8a-i) and Ti/Ag groups (Figure 8a-ii) have a similar amount of BI, as confirmed by micro-CT quantification (Figure 8b). These results demonstrate that the nanolayer silver coating does not cause a marked unfavorable response in the volume of newly regenerated bone.

3. Discussion

Titanium and titanium alloys are the most widely chosen biomaterial for orthopedic implants due to their intrinsic properties: these include lightness, high compressive/tensile strength, and biocompatibility. These materials are also compatible with rapid 3D manufacturing techniques such as SLM. Due to the large numbers of joint replacements carried out worldwide, implant failure as a result of osteolytic infection, which constitutes around 2% of all procedures, poses a serious postsurgical issue.[4,2] Consequently, there is an urgent need to find a translatable, reliable method of surface modification for titanium orthopedic materials that can reduce surface colonization,

 © 2017 The Authors. Published by WILEY-VCH Verlag GmbH & Co. KGaA, Weinheim

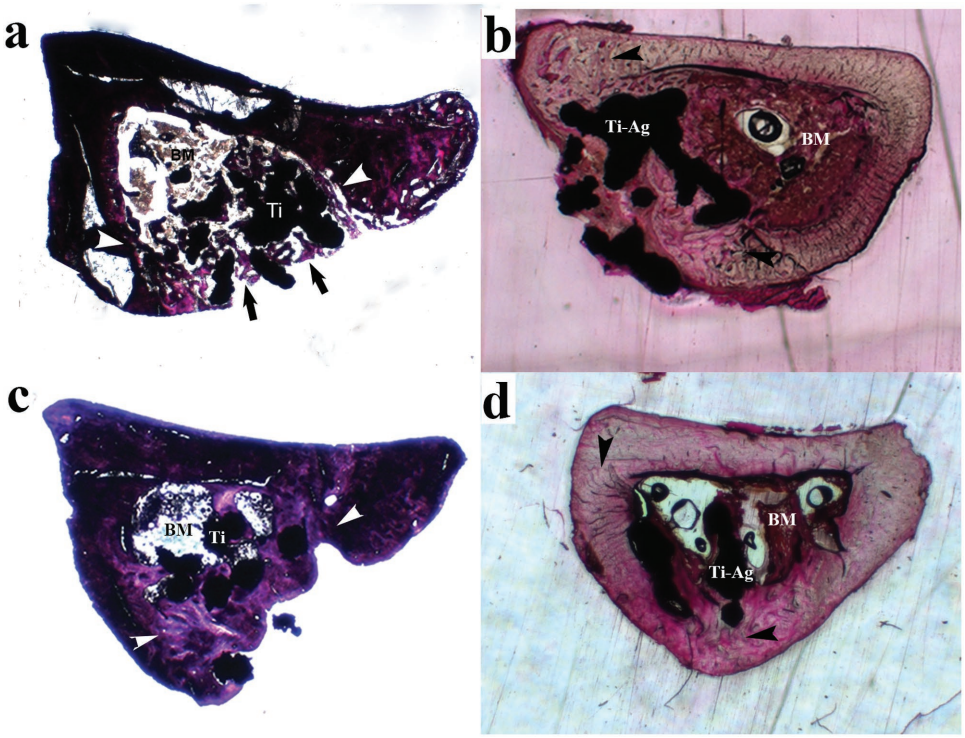

Figure 7. Light microscopic images of hematoxylin and eosin stained (50–100 mm thick) transverse sections from rat tibiae sampled at a,b) 2 or b,d) 12 weeks after implantation with either a,c) titanium or b,d) nanolayer silver-coated titanium. At 2 weeks, clear evidence of early bone deposition and dense connective tissue is seen surrounding the implants (between the black arrowheads). By 12 weeks, there is a high proportion of bone within the lesion and it is in close apposition to the struts in both types of implant. Ti, titanium only; Ti/Ag, nanolayer-coated titanium; BM, bone marrow. Monofilament suture used to secure muscle layers over implant (white arrows in a).

while preserving their osteoconductive properties.[33,34,59] One approach explored to reduce bacterial colonization and proliferation is the introduction of metallic elements to modify the surface of biomaterials. A variety of metals have been explored in this field, including zinc,[35] strontium,[36] gallium,[59] and gold/palladium[37] although silver is the most widely employed metal coating on materials surfaces due to its antimicrobial properties and the susceptibility of multidrug resistant bacterial strains to silver.[9,33]

In terms of antimicrobial coatings on bone implants, ALD offers the prospect of producing ultrathin, highly conformal coatings on all wettable surfaces of the implant.[28,38] One of the key advantages of using ALD to coat the implants is that under appropriate conditions, it proceeds via saturative steps, resulting in self-limiting film growth. This means that ALD can give truly atomic scale control of the deposition process and can produce ultrathin films with excellent uniformity and conformity, even on complex high aspect ratio 3D structures.[39] The coating we describe in this study is so thin that the total quantity of active material is kept to a minimum (below levels of detection by ICP-MS in our study), which helps to reduce concern relating to systemic toxicity of nanolayer silver-coated orthopedic implants.[40,41]

The majority of studies examining the antimicrobial potential of silver for dental/orthopedic applications rely on dissolution of Ag particles from either cements[9,42] or surface coatings[36,41,43,44] for titanium. These studies generally report a >2 log-fold increase in microbicidal activity, although silver particles are highly mobile and potentially toxic, with their tissue accumulation characteristics being largely unexplored.[40,41] Investigation of silver-nanoparticle films that are bonded to titanium is therefore of great interest as a method for reduction of postsurgical osteolytic infections, while preventing the release of potentially toxic quantities of silver. Metallic silver is inert in the body but has been demonstrated to ionize to the Ag^+ active form in the presence of moisture and body fluids, whereupon it binds to bacterial cell walls leading to cell death.[22] The mechanism of action of these Ag^+ ions has been linked to their interaction with thiol (sulfhydryl) groups. However, other target sites principally on the bacterial cell wall may be involved in the microbicidal activity of Ag[24] and Cu[45] by rupturing cell membranes and generating reactive oxygen species. The ability of Ag^+[17] or Cu^{2+} ions to exert a microbicidal effect similar to the biofilm reduction and growth inhibition we describe is dependent on the lability of the complexed metal. The majority of approaches for dissolution of Ag^+ or Cu ions for antimicrobial applications is directed toward localized release via gradual solubilization. Although localized release of Ag-nanoparticles via dissolution achieves excellent antimicrobial effects in vitro[9,42] and in vivo,[41,43,46] this approach is associated with increased silver levels in both serum and systemic organs in addition to evidence of toxicity.

Our results conclusively demonstrate that conformal nanotextured silver films, which are bonded to the titanium, reduce

 © 2017 The Authors. Published by WILEY-VCH Verlag GmbH & Co. KGaA, Weinheim

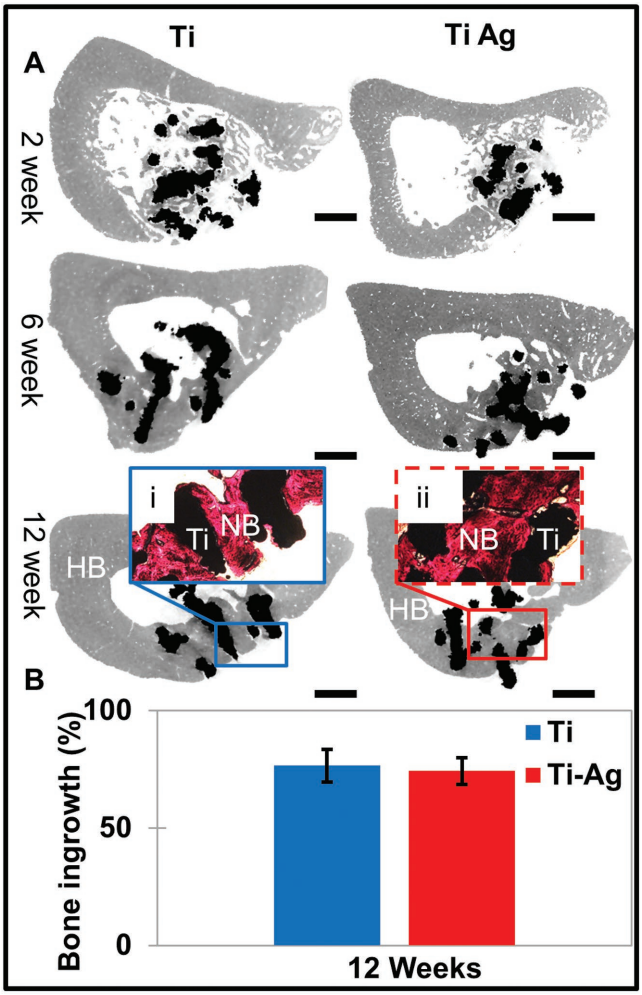

Figure 8. a) Representative micro-CT images of uncoated (Ti) and silver-coated titanium scaffold (TiAg) at 2, 6, and 12 weeks postimplantation. At 12 weeks postimplantation, inset histology image (i, ii) shows comparable amount of newly formed bone ingrowth in both groups (NS; $p > 0.05$), as confirmed by quantitative study of b) micro-CT data. Ti, titanium insert, NB, new bone; HB, host bone; Bar = 1 mm.

the growth of the osteolytic pathogen *S. epidermidis* on the surface of Ti/Ag scaffolds by over 2 log-fold. However, this response was organism specific, as MRSA growth while generally slow on Ti-only scaffolds (and similar to growth of *S. epidermidis* on Ti/Ag scaffolds) was not further inhibited by incubation on Ti/Ag scaffolds. This observation is consistent with that reported for Ag coatings of endotracheal tubes where MRSA growth is also not inhibited (in comparison to uncoated samples) over a period of 5 d.[47]

Similar to the results we report for nanolayer ALD-coated titanium implants, there is robust in vitro growth and differentiation of osteogenic cells (including mesenchymal stem cells, osteoblasts, and osteoclasts) on scaffold surfaces coated with either silver or silver composites.[14,30,31] More specifically, we examined the growth of SAOS-2 cells (an osteoblasts-like human cell line) on scaffolds between 6 and 48 h following culture and show ultrastructural evidence of cell survival and adherence, in addition to an MTT assay confirming cell population viability on both Ti-only and Ti/Ag scaffolds. Our findings are consistent with both human SAOS-2 cell and mouse osteoblast cells (MC3T3-E1)[43,48] grown on silver-nanoparticle-coated titanium surfaces.[59] However, in vitro responses can be cell type specific as high concentrations of labile Ag-containing surface coatings are known to be toxic to human fetal osteoblasts.[49] We also found that both attachment and growth of HDMEC is well tolerated on Ag-coated surfaces, similar to that described for human umbilical vein endothelial cells grown on silver-doped ceramic nanopowder.[50] In a mouse model where higher concentrations of Ag-nanoparticles are released into the microcirculation, significant toxicity on endothelium has also been reported.[51] We also observed that two other human cell lines (Hs27 and HaCaT; data not shown) show robust cell growth on Ti/Ag scaffolds, consistent with observations that growth of a variety of cell types[52] on titanium surfaces coated with various silver compositions is supported.

The in vivo studies are the first to document the relationship between pre-existing bone, neovascularization (new blood vessel growth), osteogenesis, and remodeling during the 12 week time frame of a solid uncoated or ALD-nanolayer-coated implant. These unique observations on SEM of vascular casts of tibial samples show robust new capillary formation by 2 weeks postimplantation, particularly around the struts of the scaffolds, with numerous small caliber vessels emerging from the surrounding periosteum and forming irregular interconnected networks. The presence of numerous highly branched capillaries emerging from pre-existing vessels is a well-recognized process in the cortical bone regeneration process,[53,54] however, we are unaware of their demonstration in the context of solid (particularly titanium) implants. These capillary networks precede mature bone ingrowth into the scaffolds at 2 weeks and are most likely associated with the significant increase in gene expression associated with implantation of roughened titanium surfaces.[55]

We also detail the first ultrastructural evidence for de novo formation of Haversian systems directly on the surface of a 2 week postimplantation Ti/Ag scaffold; similar to a report in which Sr/Ag-doped nanotubules induce osteogenesis in vivo.[36] Porous scaffolds with roughened surfaces (similar to both Ti-only and Ti/Ag implants described in our study) provide morphology similar to trabecular bone, to which osteoblasts can attach in vitro and in vivo, differentiate and deposit matrix that will eventually mineralize and begin the formation of woven bone.[56] By 12 weeks' postimplantation, there is clear evidence of bone and vascular remodeling within the porous structure of Ti-only and Ti/Ag scaffolds, including Volkmann's canals with attendant capillaries—features that are characteristic of mature bone growth.[54,57] In addition, 2D light microscopic examination of thick histological sections and 3D X-ray computed microtomographic reconstructions revealed excellent bone ingrowth in both Ti-only and Ti/Ag scaffolds, similar to that described for rats implanted with titanium coated with either silver-oxide-doped hydroxyapatite[43] or silver-impregnated nanotubes.[17]

4. Conclusion

We have demonstrated the SLM manufacture of bespoke of titanium scaffolds, which have been coated by the ALD

 © 2017 The Authors. Published by WILEY-VCH Verlag GmbH & Co. KGaA, Weinheim

process with a uniform, conformal nanolayer of silver. Silver-nanoparticle-coated SLM titanium scaffolds induce a 2-log fold reduction in surface growth of a major osteolytic pathogen by (*S. epidermidis*), as well as supporting robust growth and differentiation of human cell lines important for bone regeneration. In addition, we show for the first time that titanium implants coated with a silver nanolayer (≈40 nm) induce robust osteogenesis and angiogenesis in vivo, with no evidence of the systemic toxicity that is commonly associated with thicker coatings. Our results highlight the considerable benefits of ALD nanolayer silver-coated titanium implants warranting their further investigation for use in clinical orthopedic applications.

5. Experimental Section

Preparation of Nanolayer-Coated Titanium Scaffolds—Selective Laser Melting of Bespoke Titanium Solids and Foams: All of the SLM parts in this work were fabricated on a SLM Realizer 2 – 250 (MCP, Germany), using Realizer software (Realizer, GmbH, Borchen, Germany) for the manipulation of CAD files. Before starting the SLM manufacturing process, the chamber was flushed with Argon gas until the oxygen level was below 250 ppm. The oxygen level was determined using a Rapidox 2100 gas analyzer (Cambridge Sensotec Ltd., St Ives, UK). The flushing was stopped once the oxygen was below 250 ppm and the build process was then started. The feedstock for SLM was grade 1 commercially pure titanium powder, which was produced by a gas atomization process (Sumitomo, Japan). The feedstock had a modal particle diameter of 28.5 µm, with 90% of the particles being under 45 µm.

For the SLM of porous structures, the powder layer thickness was set at 50 µm, the laser beam diameter was 80 µm and the laser power and exposure were set to produce melt spots with a nominal diameter 180 µm. These parameters enabled the generation of porous "wire frame" structures with a nominal porosity of 65%. For the solid structures, the scanning strategy created the outer circular profile first and then filling in with hatch lines, which alternated between alignment in the *x*-direction for one build layer and alignment in the *y*-direction for the next build layer. A laser beam diameter of 80 µm with a point distance (the separation of adjacent hatch lines of 70 µm was used). The profiles were formed using 95 W of laser power with 700 µs exposures for the profiles, while the hatch pattern was formed using 165 W of laser power with 600 µs exposures.

Following manufacture, scaffolds were cleaned (to remove residual organic solvents and unsintered powder): samples were immersed in 5% micro-90 detergent (Decon, Sussex, UK) in distilled water at 60 °C and sonicated for 90 min using an ultrasonic bath (VWR, Radnor, USA). Samples were then rinsed again prior to sonication in distilled water at 70 °C for a further 90 min before a final rinse in fresh distilled water. The structures were then dried at 80 °C in an oven before being sintered at 1400 °C for 3 h in a VFS HEQ 2624 vacuum furnace (Philadelphia, USA) at a pressure of 5 Torr to increase compressive strength and reduce the quantity of incipiently melted powder particles. Prior to ALD, sintered solid and porous structures were cleaned again by repeating the process described above. To ensure consistency in scaffolds used throughout the experiments described in this study, 2400 samples were fabricated in a single batch (1200 solid and 1200 foam structures) and used for all subsequent experiments described in this study.

Preparation of Nanolayer-Coated Titanium Scaffolds—Atomic Layer Deposition of Silver: Silver was deposited on half the total number of solid and porous implants by direct liquid injection ALD using an Aixtron AIX200FE reactor, which was customized as described in ref. [58]. The self-limiting ALD process used for the deposition of silver has previously been reported.[28] A 0.1 molar solution of (hexafluoroacetylacetonato) silver(I)(1,5-cyclooctadiene) (hfac)Ag(1,5-COD) (SAFC Hitech, Bromborough, UK) in anhydrous toluene (Sigma-Aldrich, Germany) was used as the silver source. Hig performance liquid chromatography (HPLC) grade Propan-1-ol (Fisher, Leics, UK) was use as a coreactant and was delivered into the reactor using a conventional vapor-draw source held at room temperature (≈20 °C). During each ALD cycle, (hfac)Ag(1,5-COD) solution was introduced into the reactor for 4 s at a rate of 17.5 µL s^{-1} and was volatilized using a vaporizer set to 130 °C. The vapor was transported from the vaporizer into the reactor chamber using 200 sccm of argon (99.999%; BOC, UK) carrier gas. The coreactant was introduced directly into the reactor for 4 s via a Swagelok ALD valve. During each ALD cycle, the two reactants were sequential pulses into the reactor with 8 s gas purges between them to prevent reactions in the gas phase. To coat the SLM titanium implants, samples were mounted in a custom-made titanium holder and the ALD sequence was repeated 500 times. To ensure that growth on the implant structures proceeded in a self-limiting fashion, the reactor temperature was adjusted slightly until a low mass thermocouple attached to the top of one of the implants read 125 °C (the midpoint of the self-limiting ALD temperature window).[28]

The microstructure and morphology of the silver films were investigated using XRD and SEM. XRD was carried out on silver films deposited on Si(100) wafers (virgin test grade supplied by Compart Technology Ltd., Tamworth, UK) using a Bragg-Brentano diffractometer with a Copper Kα X-ray source (Rigaku miniflex, Tokyo, Japan). Although titanium foils can be used for XRD, silicon was selected for this purpose as it avoids substrate related diffraction peaks in the region of interest, which partially obscures the silver diffraction peaks. SEM of silver deposited onto the titanium structures was carried out using a field emission gun scanning electrom microscope (JEOL JSM-7001F, Tokyo, Japan). Film composition was determined using EDX spectroscopy on coated implants as well as XPS on flat titanium witness samples. EDX was carried out using an INCA x-act detector (x-act-51-ADD0001, Oxford Instruments plc, Abingdon, UK) attached to the FEG–SEM. XPS measurements were carried using a FISONS VG Escalab MKII with an aluminum Kα X-ray source (1486.6 eV). Mass gain measurements were used to estimate the quantity of silver deposited during the ALD process. Mass gain per unit area was estimated by measuring the mass of flat titanium witness samples using a high precision analytical balance (Mettler Toledo XS-205-DU) before and after film deposition.

Preparation of Nanolayer-Coated Titanium Scaffolds—Sterilization of Solid and Porous Titanium Implants: Before use in biological assays, all samples were sterilized by immersion in 200 µL of 70% ethanol (Fisher Scientific UK Ltd, Loughborough, UK) for 2 h. The ethanol was then removed and the samples were exposed to UV radiation for 30 min on each side of implant) in a Class II biological safety cabinet; method adapted from ref. [59]

Microbiology—Bacterial Strains and Culturing: The provenance of osteolytic strains of both *S. epidermidis* (ATCC 35983[60]) as well as MRSA (*S. aureus* ATCC 43300) was confirmed by a universal 16S rRNA PCR protocol,[61] followed by DNA sequencing and confirmation of identity using the BLAST sequence algorithm[62] within the NCBI database. These organisms were grown at 37 °C under aerobic conditions on either tryptone soya agar or in tryptone soya broth (both from Oxoid Ltd., Hampshire, UK) with shaking at 150 rpm. A calibration graph for both microorganisms was constructed by means of dilution series plating of cultures at regular points throughout growth and then plotting cfu mL^{-1} versus OD_{660}. This calibration was repeated in triplicate and for experimental purposes, a final loading of $\approx 1 \times 10^3$ cells per scaffold was used via serial dilution of fresh cultures in tryptic soy broth (TSB). Cell loadings in these experiments were confirmed and verified using dilution plate counts.

Microbiology—Assessing Bacterial Biofilm Formation on Solid Titanium Implants: To seed *S. epidermidis* onto solid titanium implants, an overnight culture was serially diluted to a final concentration of 5×10^5 cells mL^{-1}, and 2 µL of this suspension was applied to the surfaces of either the control titanium (Ti-only) or ALD prepared nanolayer silver scaffolds (Ti/Ag; a nominal coating thickness of ≈13 nm) solid titanium scaffold, which were located in a 96-well culture plate. The samples were

 © 2017 The Authors. Published by WILEY-VCH Verlag GmbH & Co. KGaA, Weinheim

then incubated overnight at 4 °C to allow bacterial attachment, and the following day 100 µL of fresh TSB broth was gently added to avoid shear stress on the organisms. The samples ($n = 6$ replicates per group) were then further incubated at 37 °C for 96 h. Microbial biofilms were assessed by the widely employed crystal violet staining method. Briefly, Ti scaffolds were recovered and following washing in distilled water, the implants were then allowed to dry at room temperature overnight prior to being stained with 1% CV (Sigma-Aldrich, UK) in water for 45 min. The excess dye was removed by washing the implants with distilled water. Elution of crystal violet stain was performed by adding a 150 µL volume of 95% ethanol with shaking, to dislodge the attached cells. The implant was removed prior to measuring the absorbance of the solubilized crystal violet at OD_{595} in a spectrophotometric plate reader (Flurostar Omega: BMG Labtech). All experiments were repeated three times and a single representative data set presented.

Microbiology—Bacterial Recovery from Titanium Scaffolds: Unless otherwise indicated, all materials were purchased from Sigma-Aldrich, UK. Total bacterial counts were used to estimate the number of viable organisms remaining on the implants. After 96 h, implants with adherent bacteria were gently washed in sterile phosphate buffered saline (PBS) and transferred into a 1.5 mL microcentifuge tube. A 1 mL volume of sterile of Ringers' solution (Oxoid Ltd., Hampshire, UK) was added to the sample and the bacteria were recovered by vortex mixing for 5 min. Following bacterial recovery, the washed implants were then stained with 1% (w/v) crystal violet (as above) to assess the numbers of organisms remaining on the implants. The recovered viable bacteria in Ringers' were enumerated by serial dilution on Tryptone soya agar plates. The plates were subsequently incubated for 24 h at 37 °C and the colonies counted.

Cell Culture—Seeding Cells on Implants: Solid implants were immersed in 1 mL of serum free Dulbecco's Modified Eagle's Medium (DMEM) media and subsequently vacuum processed at 10 psi for 15 min to remove air bubbles and wet the entire implant surface. The implants were then incubated in a humidified incubator at 37 °C with 5% CO_2 for a further 3 d in DMEM media supplemented with 10% fetal bovine serum (FBS; both from Gibco, UK).

Prior to seeding cells on the implants, SAOS-2 (osteoblast-like), HDMEC (endothelial), HaCaT (keratinocyte), and Hs27 (fibroblast) cells were cultured in media consisting of DMEM supplemented with 10% heat-inactivated FBS and maintained in a humidified incubator at 37 °C and 5% CO_2. A total of 2 µL of cell suspension containing 5×10^3 cells were pipetted onto the surface and the implants further incubated for 30 min to allow cells to adhere to the scaffold surface. To avoid shear stress on the adherent cells, 400 µL of prewarmed media (DMEM with 10% FBS) was gently added to the culture plate. The implants were then incubated for either 6, 24, or 48 h ($n = 4$ per group) before preparation for ultrastructural analyses.

In Vivo Model of Bone Regeneration: The animal experiments described in this study were approved by both the local animal care committee (Ulster University) as well as national authority (UK Home Office) and were carried out in strict adherence to guidelines for the use of experimental animals. In brief, a group of 10–12 week old male Wistar rats (300–400 g body weight) were appropriately anesthetized and prepared for surgery, prior to drilling a 2.5 mm diameter subcritical defect in the mid shaft of the medial face of right tibia as previously described.[63,64] During surgery, rats were randomly assigned to receive either a single Ti or Ti–Ag scaffold (12 per group) and the implant was press fitted into the defect. Animals were euthanized at either 1, 2, 3, 4, 6, or 12 weeks after surgery.

In Vivo Detection of Ag Using ICP-MS: The rats implanted with either Ti-only or Ti/Ag foams in the tibia (see above) were left for 12 weeks and following euthanasia, livers harvested to determine the quantity of accumulated silver by ICP-MS. In preparation for determination of free silver content, 250 mg of bovine liver (as a control) and 500 mg rat liver were freeze-dried and powdered prior to mixing in a final volume of 50 mL in double-distilled water. The tissues were then digested by microwaving: each sample was placed in a digest tube to which 4 mL of HNO_3 and 1 mL of H_2O_2 were added, before being microwaved for 120 s. A 1 mL volume of concentrated HCl was then added to each tube. The contents of the digest tubes were decanted into a 50 mL tubes and samples were autoloaded and analyzed for Ag concentration using an Elan 6100 ICP-MS equipment (Perkin-Elmer SCIEX, Norwalk, CT, USA). This was calibrated using Aristar ICP-MS multielement standards and single element standards (Merck BDH), diluted in 3.5% v/v HNO_3 and 0.5% v/v HF. Blanks, Ag-spiked samples, and bovine liver were used reference points and standards in addition to the normal ICP-MS standard operating procedure standards.

X-Ray Computed Microtomography: For the 2, 6, and 12 weeks postsurgical samples, the tibiae from rats with either Ti-only or Ti/Ag implants were harvested, immersed in 10% buffered formal saline solution and dissected for micro-CT (μCT) scanning as previously described.[64] An 85 kV, 111 µA source current was employed in the experiment and a total of 1000 projections were acquired. X-rays were filtered using a 0.5 mm thick copper filter to minimize beam-hardening effects. The scans were reconstructed using commercial software (Datos|x rec, Phoenix|X-ray General Electric Company, Measurement and Control) according to the manufacturer's instructions. The reconstructed images were visualized using Avizo Image processing software (Visualisation Sciences Group, Merignac Cedex, France). The defect region was identified and bone ingrowth quantified, using an in-house algorithm as described in ref. [63] The percentage of bone ingrowth was calculated for the 12 week samples ($n = 6$ for each group) to investigate the biological effect of silver coating at the end point of the experiment.

X-Ray Computed Microtomography—Histology: Following XMT, the tibial samples were decalcified in a solution of 14% ethylenediaminetetraacetic acid (EDTA; Sigma-Aldrich, Dorset, UK) in PBS (pH 7.4), with the EDTA being changed every 2–3 d for 3 weeks. The samples were then processed for embedding in LR white (TAAB Laboratories Equipment Ltd, Berks, UK); in brief, samples were successively dehydrated in two changes of 70% ethanol (overnight), two changes of 80% ethanol (1.5 h each), 2 changes of 90% ethanol (1.5 h each) and 3 changes of 100% ethanol (twice for 1.5 h each and one overnight). Samples were then infiltrated with a mixture of 50% ethanol/50% LR white (TAAB Laboratories Equipment Ltd., Berks, UK) overnight, followed by infiltration with 100% LR white for 24 h. To initiate hardening of the resin, 20 µL of accelerator (TAAB Laboratories Equipment Ltd, Berks, UK) was added to 10 mL LR white and the tibial sample was critically orientated in a clear base mold (Surgipath, Leica, Milton Keynes, UK) prior to polymerization at 4 °C for 2 h. Excess resin was ground from the sample and the trimmed blocks were glued onto plastic microscope slides (EXAKT, Oklahoma City, USA) with Krazy Glue (Westerville, USA) and UV treated for 5 min using a EXAKT vacuum adhesive press (EXAKT, Oklahoma City, Oklahoma, USA). Samples were cut ≈1 mm from the center of the titanium scaffold using a diamond band cutter and subsequently ground with K400, K1200, and K4000 grinding paper (all from EXAKT, Oklahoma City, USA) to yield 50–100 µm thick sections for staining and microscopic evaluation.

Sections were stained with Gill's hematoxylin as follows: sections were placed in 1% formic acid (Sigma-Aldrich, Dorset, UK) for 10 min, rinsed in absolute ethanol for 5 min, and rinsed in deionized water for 2 min. Hematoxylin solution (Sigma-Aldrich, Dorset, UK) was applied dropwise onto the section, allowed to stain for 30 min and then sections were thoroughly rinsed in tap water. Multiple stain solution (Polysciences Inc., Warrington, USA) was added for 20 min followed by another rinse in tap water and air drying. Stained samples were then examined on a Zeiss Axiophot microscope (Zeiss; Wetzlar, Germany) at a range of objective magnifications.

Vascular Casting: To examine vascular ingrowth into the titanium scaffolds, a number of rats were injected intraperitoneally with 2400 U kg^{-1} body weight of porcine heparin (Sigma-Aldrich, UK) 30 min before the casting procedure to inhibit clotting in the microvasculature. Prior to perfusion, animals were anesthetized with a mixture of Ketamine and Xylazine as described above. After confirmation of a deep plane of anesthesia, an incision was made in the midline of the abdomen and the

 © 2017 The Authors. Published by WILEY-VCH Verlag GmbH & Co. KGaA, Weinheim

descending aorta exposed and tied off proximally. A catheter was inserted into the descending aorta secured using 4-0 Ethicon Ethilon polyamide (Johnson & Johnson, New Brunswick, New Jersey, USA) and, the inferior vena cava severed. The vasculature was flushed with 25 mL saline (warmed to 37 °C) followed by 25 mL of 2.5% PBS (pH 7.4) buffered glutaraldehyde warmed to 37 °C. Finally, a volume of 25 mL Pu4ii resin (vasQtec, Zurich, Switzerland) was injected into the circulation and the resin allowed to harden at room temperature overnight prior to storage at –20 °C. The tibiae were subsequently harvested from animals by careful dissection, immersed in tap water, and subsequently stored at –20 °C prior to maceration. Samples were macerated in 20 mL 20% NaOH (Fisher Scientific UK Limited, Leicestershire, UK) for 24 h with regular changes followed by extensive washing in distilled water a total of five times. Samples were left to dry at room temperature prior to preparation for SEM.

Preparation of Samples for SEM: Scaffolds either containing bacteria (following 96 h of incubation), those incubated with cells (6–48 h) or alternatively tibiae that had been appropriately macerated to remove all cellular material (2–12 weeks' postsurgery; see above) were washed in sterile PBS and fixed in glutaraldehyde 2.5% in 0.1 M sodium–cacodylate buffer (pH7.4) either overnight or until processing for SEM. The samples were then washed gently three times (for 10 min each) in 1 mL of 0.1 M sodium–cacodylate buffer and dehydrated in ascending grades of ethanol (25%, 50%, 75%, 95%, and 100%; Sigma, UK). Following dehydration, samples were then immersed in hexameythldisilazane (Sigma, UK) for 10 min, before removal, air drying and subsequent mounting on aluminum stubs. Prior to ultrastructural examination, samples were sputter coated with gold-palladium (Polar ES100; set at 18 mA for 240 s) and imaged with a scanning electron microscope (JEOL; Japan) at accelerating voltage of 10kV and a spot size of 25 µm.

Statistical Analyses: For each microbiological (n = 6 replicates; experiment repeated three times) or cell culture assay (n = 4; no repeats); individual representative experiments are shown in the results section. All data sets were analyzed with the aid of GraphPad Prism6 software (Intuitive Software for Science, San Diego, USA). Results are expressed as mean ± standard error. Significance was determined using Independent two-tailed t-tests for group comparisons, with $p < 0.05$ considered significant.

Acknowledgements

A.D.-M. and N.M.T. contributed equally to this work. The tomography work was made possible by the facilities and support provided by the Research Complex at Harwell (RCaH), funded in part by the EPSRC (EP/I02249X/1). The AgNP ALD work was partly funded by EPSRC through the Liverpool knowledge transfer account (EP/H500146/1). This work was supported in part by funding from the EPSRC Centre for Laser Based Production Processes, grant EP/K030884. Each of the authors of this manuscript state that they have no conflict of interest to declare.

Received: January 10, 2017
Revised: February 1, 2017
Published online:

[1] U. Geipel, M. Herrmann, *Orthopade* **2004**, *33*, 1411.
[2] R. Schwarzkopf, R. C. Takemoto, I. Immerman, J. D. Slover, J. A. Bosco, *J. Bone Jt. Surg., Am. Vol.* **2010**, *92*, 1815.
[3] A. B. Pedersen, J. E. Svendsson, S. P. Johnsen, A. Riis, S. Overgaard, *Acta Orthop.* **2010**, *81*, 542.
[4] E. F. Berbari, A. D. Hanssen, M. C. Duffy, J. M. Steckelberg, D. M. Ilstrup, W. S. Harmsen, D. R. Osmon, *Clin. Infect. Dis.* **1998**, *27*, 1247.
[5] W. Zimmerli, P. E. Ochsner, *Infection* **2003**, *31*, 99.
[6] S. Nishimura, T. Tsurumoto, A. Yonekura, K. Adachi, H. Shindo, *J. Orthop. Sci.* **2006**, *11*, 46.
[7] A. G. Gristina, P. Naylor, Q. Myrvik, *Med. Prog. Technol.* **1988**, *14*, 205.
[8] D. Hudetz, E. Rod, A. Radic, A. Ivkovic, *Medicinski Glasnik* **2012**, *9*, 152.
[9] V. Alt, T. Bechert, P. Steinrucke, M. Wagener, P. Seidel, E. Dingeldein, E. Domann, R. Schnettler, *Biomaterials* **2004**, *25*, 4383.
[10] M. M. Tunney, G. Ramage, S. Patrick, J. R. Nixon, P. G. Murphy, S. P. Gorman, *Antimicrob. Agents Chemother.* **1998**, *42*, 3002.
[11] a) M. Schafroth, W. Zimmerli, P. E. Ochsner, *Praxis* **1999**, *88*, 2101; b) T. P. Schmalzried, *J. Arthroplasty* **2006**, *21*, 97.
[12] X. Wang, S. Xu, S. Zhou, W. Xu, M. Leary, P. Choong, M. Qian, M. Brandt, Y. M. Xie, *Biomaterials* **2016**, *83*, 127.
[13] C. Mao, H. Li, F. Cui, Q. Feng, C. Ma, *J. Mater. Chem.* **1999**, *9*, 2573.
[14] J. Raphel, M. Holodniy, S. B. Goodman, S. C. Heilshorn, *Biomaterials* **2016**, *84*, 301.
[15] S. Verrier, M. Peroglio, C. Voisard, B. Lechmann, M. Alini, *Biomaterials* **2011**, *32*, 672.
[16] G. Xu, X. Shen, L. Dai, Q. Ran, P. Ma, K. Cai, *Mater. Sci. Eng., C* **2017**, *70*, 386.
[17] H. Cheng, Y. Li, K. Huo, B. Gao, W. Xiong, *J. Biomed. Mater. Res., Part A* **2014**, *102*, 3488.
[18] E. Sudmann, H. Vik, M. Rait, K. Todnem, K. J. Andersen, K. Julsham, O. Flesland, J. Rungby, *Med. Prog. Technol.* **1994**, *20*, 179.
[19] G. Josefsson, G. Gudmundsson, L. Kolmert, S. Wijkstrom, *Clin. Orthop. Relat. Res.* **1990**, *253*, 173.
[20] J. W. Alexander, *Surg. Infect.* **2009**, *10*, 289.
[21] A. D. Russell, W. B. Hugo, *Prog. Med. Chem.* **1994**, *31*, 351.
[22] A. B. Lansdown, *J. Wound Care* **2002**, *11*, 125.
[23] H. Liedberg, T. Lundeberg, *Br. J. Urol.* **1990**, *65*, 379.
[24] W. K. Jung, H. C. Koo, K. W. Kim, S. Shin, S. H. Kim, Y. H. Park, *Appl. Environ. Microbiol.* **2008**, *74*, 2171.
[25] C. M. Tilmaciu, M. Mathieu, J. P. Lavigne, K. Toupet, G. Guerrero, A. Ponche, J. Amalric, D. Noel, P. H. Mutin, *Acta Biomater.* **2015**, *15*, 266.
[26] H. Cao, X. Liu, F. Meng, P. K. Chu, *Biomaterials* **2011**, *32*, 693.
[27] M. Leskela, M. Ritala, *Angew. Chem., Int. Ed.* **2003**, *42*, 5548.
[28] Z. Golrokhi, S. Chalker, C. J. Sutcliffe, R. J. Potter, *Appl. Surf. Sci.* **2016**, *364*, 789.
[29] a) L. Mullen, R. C. Stamp, W. K. Brooks, E. Jones, C. J. Sutcliffe, *Appl. Biomater.* **2009**, *89*, 325; b) L. Mullen, R. C. Stamp, P. Fox, E. Jones, C. Ngo, C. J. Sutcliffe, *Appl. Biomater.* **2010**, *92*, 178.
[30] A. Ewald, S. K. Gluckermann, R. Thull, U. Gbureck, *Biomed. Eng. Online* **2006**, *5*, 22.
[31] L. Zhao, P. K. Chu, Y. Zhang, Z. Wu, *Appl. Biomater.* **2009**, *91*, 470.
[32] B. S. Smith, S. Yoriya, T. Johnson, K. C. Popat, *Acta Biomater.* **2011**, *7*, 2686.
[33] A. Besinis, T. De Peralta, R. D. Handy, *Nanotoxicology* **2014**, *8*, 745.
[34] J. Chen, R. A. Bly, M. M. Saad, M. A. AlKhodary, R. M. El-Backly, D. J. Cohen, N. Kattamis, M. M. Fatta, W. A. Moore, C. B. Arnold, M. K. Marei, W. O. Soboyejo, *Mater. Sci. Eng. C* **2011**, *31*, 826.
[35] G. Jin, H. Qin, H. Cao, S. Qian, Y. Zhao, X. Peng, X. Zhang, X. Liu, P. K. Chu, *Biomaterials* **2014**, *35*, 7699.
[36] H. Cheng, W. Xiong, Z. Fang, H. Guan, W. Wu, Y. Li, Y. Zhang, M. M. Alvarez, B. Gao, K. Huo, J. Xu, N. Xu, C. Zhang, J. Fu, A. Khademhosseini, F. Li, *Acta Biomater.* **2016**, *31*, 388.
[37] S. Svensson, F. Suska, L. Emanuelsson, A. Palmquist, B. Norlindh, M. Trobos, H. Backros, L. Persson, G. Rydja, M. Ohrlander, B. Lyven, J. Lausmaa, P. Thomsen, *Nanomedicine* **2013**, *9*, 1048.
[38] M. Ritala, K. Kukli, A. Rahtu, P. I. Raisanen, M. Leskela, T. Sajavaara, J. Keinonen, *Science* **2000**, *288*, 319.

 © 2017 The Authors. Published by WILEY-VCH Verlag GmbH & Co. KGaA, Weinheim

[39] M. Ritala, M. Leskela, J. P. Dekker, C. Mutsaers, P. J. Soininen, J. Skarp, *Chem. Vap. Deposition* **1999**, *5*, 7.
[40] S. Qiao, H. Cao, X. Zhao, H. Lo, L. Zhuang, Y. Gu, J. Shi, X. Liu, H. Lai, *Int. J. Nanomed.* **2015**, *10*, 653.
[41] M. Tsukamoto, H. Miyamoto, Y. Ando, I. Noda, S. Eto, T. Akiyama, Y. Yonekura, M. Sonohata, M. Mawatari, *Biomed. Res. Int.* **2014**, *2014*, 902343.
[42] P. Prokopovich, M. Kobrick, E. Brousseau, S. Perni, *Appl. Biomater.* **2015**, *103*, 273.
[43] S. Eto, H. Miyamoto, T. Shobuike, I. Noda, T. Akiyama, M. Tsukamoto, M. Ueno, S. Someya, S. Kawano, M. Sonohata, M. Mawatari, *J. Orthop. Res.* **2015**, *33*, 1391.
[44] P. Khalilpour, K. Lampe, M. Wagener, B. Stigler, C. Heiss, M. S. Ullrich, E. Domann, R. Schnettler, V. Alt, *Appl. Biomater.* **2010**, *94*, 196.
[45] M. Li, Z. Ma, Y. Zhu, H. Xia, M. Yao, X. Chu, X. Wang, K. Yang, M. Yang, Y. Zhang, C. Mao, *Adv. Healthcare Mater.* **2016**, *5*, 557.
[46] T. Akiyama, H. Miyamoto, Y. Yonekura, M. Tsukamoto, Y. Ando, I. Noda, M. Sonohata, M. Mawatari, *J. Orthop. Res.* **2013**, *31*, 1195.
[47] K. M. Tarquinio, N. K. Kothurkar, D. Y. Goswami, R. C. Sanders Jr., A. L. Zaritsky, A. M. LeVine, *Int. J. Nanomed.* **2010**, *5*, 177.
[48] a) Y. Liu, Z. Zheng, J. N. Zara, C. Hsu, D. E. Soofer, K. S. Lee, R. K. Siu, L. S. Miller, X. Zhang, D. Carpenter, C. Wang, K. Ting, C. Soo, *Biomaterials* **2012**, *33*, 8745; b) S. H. Uhm, D. H. Song, J. S. Kwon, S. B. Lee, J. G. Han, K. N. Kim, *Appl. Biomater.* **2014**, *102*, 592.
[49] B. S. Necula, J. P. van Leeuwen, L. E. Fratila-Apachitei, S. A. Zaat, I. Apachitei, J. Duszczyk, *Acta Biomater.* **2012**, *8*, 4191.
[50] R. B. Bostancioglu, C. Peksen, H. Genc, M. Gurbuz, F. B. Karel, A. S. Koparal, A. Dogan, N. Kose, A. T. Koparal, *Biomed. Mater.* **2015**, *10*, 045024.
[51] H. Guo, J. Zhang, M. Boudreau, J. Meng, J. J. Yin, J. Liu, H. Xu, *Part. Fibre Toxicol.* **2016**, *13*, 21.
[52] a) A. Cochis, B. Azzimonti, C. Della Valle, R. Chiesa, C. R. Arciola, L. Rimondini, *J. Biomed. Mater. Res., Part A* **2015**, *103*, 1176; b) S. Nath, S. Kalmodia, B. Basu, *J. Mater. Sci.: Mater. Med.* **2010**, *21*, 1273; c) E. Verne, M. Miola, C. V. Brovarone, M. Cannas, S. Gatti, G. Fucale, G. Maina, A. Masse, S. Di Nunzio, *J. Mater. Sci. Mater. Med.* **2009**, *20*, 733.
[53] I. H. Choi, J. H. Ahn, C. Y. Chung, T. J. Cho, *J. Orthop. Res.* **2000**, *18*, 698.
[54] U. E. Pazzaglia, T. Congiu, F. Ranchetti, M. Salari, C. Dell'Orbo, *Anat. Sci. Int.* **2010**, *85*, 31.
[55] N. Donos, M. Retzepi, I. Wall, S. Hamlet, S. Ivanovski, *Clin. Oral Implants Res.* **2011**, *22*, 390.
[56] a) C. S. Chang, C. Y. Su, T. C. Lin, *J. Biomed. Mater. Res.* **1999**, *48*, 411; b) Y. W. Gung, C. K. Cheng, C. Y. Su, *Med. Eng. Phys.* **2003**, *25*, 565; c) S. Morini, M. A. Continenza, G. Ricciardi, E. Gaudio, L. Pannarale, *Anat. Rec., Part A* **2004**, *278*, 419.
[57] U. E. Pazzaglia, G. Bonaspetti, F. Ranchetti, P. Bettinsoli, *J. Anat.* **2008**, *213*, 183.
[58] R. J. Potter, P. R. Chalker, T. D. Manning, H. C. Aspinall, Y. F. Loo, A. C. Jones, L. M. Smith, G. W. Critchlow, M. Schumacher, *Chem. Vap. Deposition* **2005**, *11*159.
[59] C. Della Valle, L. Visai, M. Santin, A. Cigada, G. Candiani, D. Pezzoli, C. R. Arciola, M. Imbriani, R. Chiesa, *Int. J. Artif. Organs* **2012**, *35*, 864.
[60] G. D. Christensen, W. A. Simpson, A. L. Bisno, E. H. Beachey, *Infecti. Immun.* **1982**, *37*, 318.
[61] J. Wagner, K. Short, A. G. Catto-Smith, D. J. Cameron, R. F. Bishop, C. D. Kirkwood, *PLoS One* **2008**, *3*, e3578.
[62] S. F. Altschul, T. L. Madden, A. A. Schaffer, J. Zhang, Z. Zhang, W. Miller, D. J. Lipman, *Nucleic Acids Res.* **1997**, *25*, 3389.
[63] H. Geng, N. M. Todd, A. Devlin-Mullin, G. Poologasundarampillai, T. B. Kim, K. Madi, S. Cartmell, C. A. Mitchell, J. R. Jones, P. D. Lee, *J. Mater. Sci.: Mater. Med.* **2016**, *27*, 112.
[64] S. Midha, T. B. Kim, W. van den Bergh, P. D. Lee, J. R. Jones, C. A. Mitchell, *Acta Biomater.* **2013**, *9*, 9169.

 © 2017 The Authors. Published by WILEY-VCH Verlag GmbH & Co. KGaA, Weinheim